Article:

Mound, JE, Davies, C and Coimbra e Silva, L (2015) Inner Core Translation and the Hemispheric Balance of the Geomagnetic Field. Earth and Planetary Science Letters, 424. 148 - 157. ISSN 0012-821X

https://doi.org/10.1016/j.epsl.2015.05.028

Inner Core Translation and the Hemispheric Balance of the Geomagnetic Field

Jon Mound[a], Chris Davies[a,b], Luis Silva[a,c]

[a]*School of Earth and Environment, University of Leeds, Leeds, UK.*
[b]*Institute of Geophysics and Planetary Physics, Scripps Institution of Oceanography, University of California at San Diego, La Jolla, CA, USA.*
[c]*School of Mathematics and Statistics, University of Glasgow, Glasgow, UK.*

Abstract

Bulk translation of the Earth's inner core has been proposed as an explanation of observed quasi-hemispheric seismic structure. An important consequence of inner core translation would be the generation of a spherical harmonic degree one heat flow anomaly at the inner core boundary (ICB) that would provide an inhomogeneous forcing for outer core convection. We use geodynamo simulations to investigate the geomagnetic signature of such heterogeneity. Strong hemispheric heterogeneity at the ICB is found to produce a hemispheric signature in both the morphology of the magnetic field and its secular variation; in particular, we note the formation of high-intensity flux patches at high-latitudes and American longitudes in our model with strong ICB heterogeneity. In our simulations, this model provides the best match to the Earth's field over the past 400 years according to previously proposed measures of field structure. However, these criteria do not include the hemispheric balance of the field. We propose new criteria to measure this balance and find that our model with strong ICB heterogeneity produces the poorest match to the hemispheric balance of the historical geomagnetic field.

Email address: J.E.Mound@leeds.ac.uk (phone +44(0)1133435216) (Jon Mound)

Resolution of the hemispheric balance of the magnetic field throughout the Holocene would provide a strong test of any proposal of rapid inner core translation.

Keywords: Geomagnetic field, Geodynamo, Inner core translation

1. Introduction

Hemispheric variations in the seismic properties of Earth's inner core (e.g. Tanaka and Hamaguchi, 1997; Niu and Wen, 2001; Waszek and Deuss, 2011; Miller et al., 2013) have been suggested to result from its bulk translation from west to east (Monnereau et al., 2010; Alboussière et al., 2010). In this scenario, the inner core melts on the leading eastern side, absorbing latent heat and producing a dense iron-rich fluid, and crystallises on the trailing western side, releasing latent heat and light elements into the overlying outer core. This translation represents a spherical harmonic degree one convective instability (Deguen et al., 2013). New estimates of the thermal conductivity of the solid, inner core (Pozzo et al., 2014) imply that purely thermal convection within the inner core is unlikely. Convection may still arise due to compositional density variations, although it is unclear whether the instability would persist to the present day (Gubbins et al., 2013; Labrosse, 2014).

If inner core translation does occur, the resultant melting-crystallising dichotomy at the inner-core boundary (ICB) will impose a heterogenous flux boundary condition on convection in the outer core. Recent studies have investigated the impact of heterogenous ICB heat flux on convection in the Earth's outer core (Davies et al., 2013; Sasaki et al., 2013) and suggested that the influence of inner core translation may be required to explain features such as quiet Pacific secular variation (SV) (Aubert et al., 2013) and persistent eccentricity of the geomagnetic dipole (Olson and Deguen, 2012). The seismic observation of inner core heterogeneity has not been definitively linked to a causal mechanism, and it is possible to explain the pattern with inner core translation in either direction (Monnereau et al., 2010; Cormier et al., 2011). In particular, Aubert et al. (2013) argue that explaining the observed patterns of SV requires a dynamo controlled from the ICB due to a combination of inner core translation (to provide the flux heterogeneity), gravitational coupling between the inner core and mantle (to maintain the orientation of the pattern), and an east to west translation (to promote geomagnetic westward drift in the Atlantic hemisphere). An east-west hemispheric difference in core flow, and hence the geomagnetic field, that persists over long times may represent a signature of inner core translation; in this work we consider the characteristics of such a signature.

In order to have an observable impact on the planet's magnetic field the inner core translation must be able to influence flow throughout the outer core, including near the core-mantle boundary (CMB). Seismic anomalies at the base of the mantle arise due to both chemical and thermal variations. Previous geodynamo simulations have shown that heterogeneous heat flux conditions imposed by the mantle on the core may have an important influence on core flow, and hence on the observed magnetic field and secular variation (e.g. Bloxham, 2000; Gibbons and Gubbins, 2000; Olson and Christensen, 2002), an effect which might obscure any signature of the boundary conditions at the ICB. Here, we investigate the influence of ICB heterogeneity on convection in the outer core, and whether this influence is detectable in the geomagnetic field, given the presence of strong CMB heterogeneity.

Due to the dynamic nature of core convection, the influence of heterogenous boundary conditions at either the ICB or CMB are more likely to be apparent in long timescale averages of the magnetic field, rather than in instantaneous snapshots. Therefore, we will consider both the characteristic structure of the ICB-driven signature, as well as the timescale over which it would be observed in the geomagnetic field. Of course, it is possible for a given ICB heterogeneity to have an observable signature that is in contradiction with the observed character of the Earth's magnetic field. Therefore, we also consider how well the models with different ICB heterogeneity strengths match observed characteristics of the modern field and its secular variation. To do this we makes use of existing measures of global field structure (Christensen et al., 2010), and propose new measures of the hemispheric structure of the field and its secular variation.

2. Methods

2.1. Numerical Simulations

We investigate the influence of CMB and ICB thermal heterogeneity in numerical geodynamo models that solve the magnetohydrodynamic equations for a Boussinesq fluid in a rotating spherical shell (Willis et al., 2007). Key model parameters are summarised in table 1, with the variables defined in table 2. On both the inner and outer boundary we impose no-slip conditions on the velocity, electrically insulating conditions for the magnetic field, and fixed heat flux thermal boundary conditions with patterns determined from seismic observations (see below). Compositional effects would introduce an additional source of buoyancy at the ICB resulting in double-diffusive convection and likely more vigorous flows. Although chemical buoyancy is likely important in the present Earth, we consider a chemically homogeneous system heated from below. In this set-up no heat sources exist in the volume making the total radial heat flux at the ICB equal to that at the CMB. Latent heat is released at the ICB and drives convection throughout the shell finally escaping the core at the CMB. This simplification allows us to focus on the effects of the heterogeneity of the forcing without double diffusive effects, allowing us to more easily compare with our previous non-magnetic results (Davies et al., 2013). The chosen values of Ekman, Rayleigh and Prandtl numbers correspond to those used in our previous study of non-magnetic convection with imposed ICB heat flux heterogeneity.

At the CMB we apply a heat flux pattern derived from a linear scaling of the S-wave velocity variations of Masters et al. (1996). The seismic velocity variations will arise from a combination of thermal and chemical contributions and the ultimate impact on CMB heat flux depends on a combination of the inferred variations in both temperature and thermal conductivity of the lowermost mantle and thus it is not possible to uniquely determine CMB heat flux from a tomography model. Our scaling from seismic velocity to heat flux variations is chosen following the work of Nakagawa and Tackley (2008) and is sufficiently large that the heterogeneous CMB boundary condition is expected to have an important influence on flow at the top of the core (in the absence of any ICB heterogeneity). The amplitude of the heterogeneous thermal boundary conditions applied at the CMB and ICB is

Table 1: Model Parameters

Parameter	Definition	Value
Ekman Number	$E = \frac{\nu}{2\Omega d^2}$	10^{-5}
Rayleigh Number	$Ra = \frac{\alpha g \beta}{2\Omega\kappa}$	$9 \times Ra_c$
Prandtl Number	$Pr = \frac{\nu}{\kappa}$	1
Roberts Number	$q = \frac{\kappa}{\eta}$	10
Radius Ratio	$r_\mathrm{i}/r_\mathrm{o}$	0.35
CMB Heterogeneity	$q_\mathrm{o}^* = \frac{q_o^{\max} - q_o^{\min}}{\bar{q}_o}$	2.3
ICB Heterogeneity	$q_\mathrm{i}^* = \frac{q_\mathrm{i}^{\max} - q_\mathrm{i}^{\min}}{\bar{q}_\mathrm{i}}$	0.023, 0.23, 4.2

measured by the peak-to-peak variations in heat flux relative to the mean, which we denote q^*.

Heterogeneous heat flux imposed at the ICB may also promote large scale flows, which have the potential to disrupt the influence of an imposed CMB heterogeneity. Our choice of ICB heterogeneity is motivated by the proposed inner-core translation, and the strength of the heterogeneity is directly related to the ratio between the translation speed and the rate of inner core growth. We impose a spherical harmonic pattern of degree and order 1, oriented such that the inner core is translating from 'west' to 'east' (i.e. heat flux is enhanced in the solidifying, quasi-western hemisphere). The orientation of the pattern is set to match the hemispherical seismic velocity structure determined by Waszek and Deuss (2011), that is, higher heat flux on the Western hemisphere with a boundary at 14 degrees East. We consider three values of q_i^* such that the heat flux heterogeneity at the ICB is weak (Model

Table 2: Definition of Variables

Variable	**Symbol**
Shell thickness	d
Gravitational acceleration	g
ICB heat flux	$q_{\rm i}$
CMB heat flux	$q_{\rm o}$
ICB radius	$r_{\rm i}$
CMB Radius	$r_{\rm o}$
Thermal expansivity	α
Background state radial temperature gradient	β
Magnetic diffusivity	η
Thermal diffusivity	κ
Viscosity	ν
Rotation rate	Ω

W), roughly equivalent (Model E), or strong (Model S), in comparison to our chosen value of q_o^*. Note that our non-dimensionalisation of $\bar{q}$ depends on the area of the boundary, and thus to apply the same $q^{\max}$ on both boundaries implies that $q_o^* = (r_o/r_\mathrm{i})^2 q_\mathrm{i}^*$. The values of q_i^* were chosen in consideration of previous non-magnetic convection modelling (Davies et al., 2013), which suggests that the ICB heterogeneity should be relatively dynamically unimportant in Model W, and potentially dominant in Model S.

In all cases the model resolution is to spherical harmonic degree and order 128. This was found to provide three orders of magnitude convergence in the magnetic fields and greater convergence in the velocity fields. Each of the simulations took approximately 0.4-0.5 million CPU hours of computation. The choice of parameters enabled us to investigate time scales that should be long enough to investigate the signatures of the heterogeneous forcing in the time average of the field, with manageable computational costs.

Comparison of the numerical simulations with the Earth requires us to re-dimensionalise time, for which there are two obvious options. Both the magnetic diffusion time scale ($\tau^\mathrm{d} = d^2/\eta$) and the advection time scale ($\tau^\mathrm{a} = d/U$, where U is a characteristic fluid velocity) have been used successfully in previous work; the ratio of the two time scales is the magnetic Reynolds number ($R_m = \tau^\mathrm{d}/\tau^\mathrm{a}$) which is on the order of 300 in our simulations. In this work we use the diffusion time scale resulting in time series of approximately 115,000 model years after removal of the initial transients. With this scaling, time averages over the full model run correspond to durations much longer than those available from current observational field models. Use of the advective scaling would result in time series of approximately 40,000 model years and does not significantly alter the discussion below. Further discussion of the merits of the two scalings can be found in, for example, Davies and Constable (2014); Olson et al. (2012). After dimensionalisation the simulation time series are divided into consecutive windows lasting 400 model years for comparison to gufm1 (Jackson et al., 2000).

2.2. Observational Field Models

In this work we are interested in comparing our simulations to the observed morphology of the geomagnetic field and its secular variation. Global time-dependent representations of the field are only available for the last 10,000 years, we do not consider variations on longer timescales. The Earth's current magnetic field and SV are well described by models derived from surface and satellite measurements, for example CHAOS4 (Olsen et al., 2014). The predominant non-dipolar features of the field are four lobes of concentrated magnetic flux located at high latitudes and both American and Australasian longitudes. Currently, secular variation is strong in the atlantic hemisphere and weak in the pacific.

The gufm1 reconstruction spans the past 400 years and shows that the present field and SV configurations are typical of that timescale (Jackson et al., 2000). Archeomagnetic and paleomagnetic data are used to produce models of the magnetic field that extend over a significant fraction of the Holocene (e.g. CALS3k.4b (Korte and Constable, 2011), PFM9k.1 (Nilsson et al., 2014), CALS10k.1b (Korte et al., 2011)). Although both the temporal and spatial resolution of Holocene models are limited compared to the historical or modern record, non-zonal field structure is detected in the time-averaged Holocene field. These patterns may be the result of boundary control on the Earth's dynamo, or an indication that the available observations do not span a sufficiently long time to remove all transient non-zonal features.

Due to its higher spatial and temporal resolution, we will mainly compare our dynamo results with gufm1. However, the continuous evolution of the Earth's magnetic field implies that the field characteristics determined using the restricted length of gufm1 may not be representative of the field on longer time scales. Since we expect the influence of boundary heterogeneity to be more visible in long time scale averages, we also consider the variation of field structure by evaluating consecutive 400-year windows extracted from the Holocene models. In particular, we consider the evolution of the hemispheric balance of the geomagnetic field over these time scales, as this balance is characteristic of strong hemispheric heterogeneity in the ICB heat flux.

3. Results

3.1. Field Structure

Figure 1 depicts the time-averaged radial magnetic field at Earth's surface for our three dynamo models. The CMB heat-flux pattern promotes downwelling under the areas of maximum heat flux; since the tomographic pattern is dominated by the Y_2^2 spherical harmonic, it is expected to create two pairs of flux patches, a feature that has been seen in previous studies (Olson and Christensen, 2002; Gubbins et al., 2007). However, our models do not show two clear pairs of patches. In particular, as the magnitude of the ICB heterogeneity is increased a single pair of high-latitude patches is clearly preferred, situated roughly over the Americas. The ICB heterogeneity promotes a quasi-hemispheric pattern of upwelling and downwelling in the time averaged flow, which tends to concentrate the downwelling near the CMB into a single longitudinal band.

We compare the structure of the magnetic fields produced by our models to that of the Earth using the criteria devised by Christensen et al. (2010). The first criterion (AD/NAD) is a measure of the field's relative axial dipole power,

$$\mathrm{AD/NAD} = \frac{P_{1,0}}{P_{1,1} + \sum_{n=2}^{8} \left(\frac{a}{c}\right)^{(2n-2)} \sum_{m=0}^{n} P_{n,m}} \,, \tag{1}$$

where a is the radius of the Earth, c the radius of the CMB, and the power at a given degree depends on the Gauss coefficients $g_{n,m}$ and $h_{n,m}$ and is defined by

$$P_{n,m} = (n+1)\left(g_{n,m}^2 + h_{n,m}^2\right) . \tag{2}$$

The second criterion (O/E) is a measure of the field's equatorial symmetry, defined as the ratio of power at the CMB between spherical harmonics in which $(n+m)$ is odd (i.e., equatorially antisymmetric structure) to those that are even (i.e., equatorially symmetric structure). The third criterion (Z/NZ) is a measure of the zonality of the field, defined as the ratio of power at the CMB in all zonal components to the power in all non-zonal components. The final criterion (FCF) is a measure of flux concentration defined by

$$\mathrm{FCF} = \frac{< B_r^4 > - < B_r^2 >^2}{< B_r^2 >^2} \,, \tag{3}$$

where $< ... >$ indicates the mean value over the area of integration, in this case the whole of the CMB.

Agreement between model and observed field is measured by comparing the values of the individual measures from model windows (Π_i) to the average

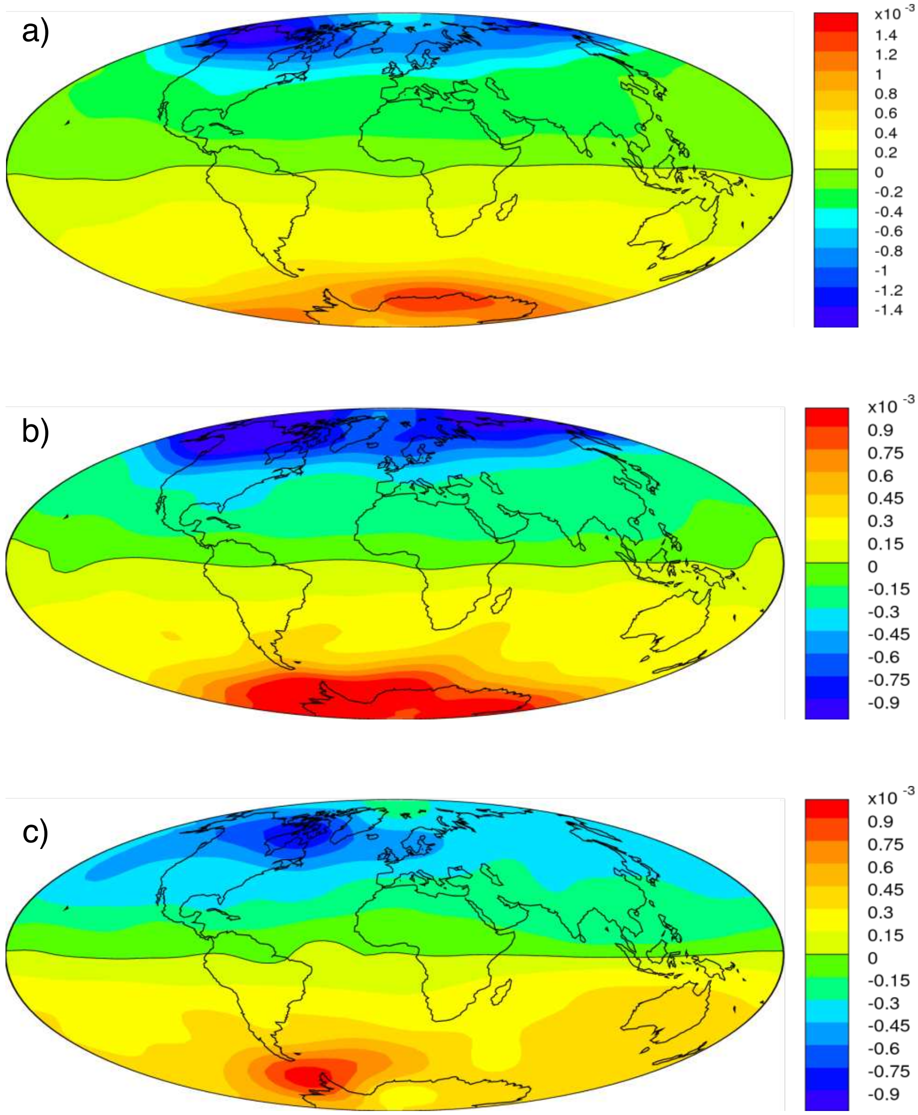

Figure 1: Time-averaged radial magnetic fields at the CMB from the dynamo models with $q_{\rm i}^*$ equal to a) 0.023, b) 0.23, and c) 4.2, all other parameters as in Table 1. Colour bars indicate dimensionless field strength. Fields are truncated at spherical harmonic degree 12.

Table 3: Field Criteria for gufm1

	AD/NAD	O/E	Z/NZ	FCF
Π^E	1.4	1.0	0.15	1.5
σ	2.0	2.0	2.5	1.75

All values from Christensen et al. (2010)

values of those measures over gufm1 (Π_i^E). The misfit of the simulations to the observed field values is measured relative to an assigned deviation for each characteristic (σ_i), and defined by a chi-squared misfit for each measure

$$\chi_i^2 = \left(\frac{\ln(\Pi_i) - \ln(\Pi_i^E)}{\ln(\sigma_i)} \right)^2 . \tag{4}$$

The model agreement with the gufm1 characteristics are deemed to be excellent, good, and marginal if the sum of the individual misfits is less than 2, 4, and 8, respectively. The values of the measures and the assigned deviations found by Christensen et al. (2010) are summarised in table 3.

The evolution of the misfit between the dynamo models and the characteristics derived from gufm1 is shown in figure 2. Model S has the best average agreement with the field structure ($\bar{\chi}^2 = 2.7$), with excellent agreement in nearly half of all windows, and at least a good agreement in 79% of the individual time windows. In comparison, model W matches the field poorly ($\bar{\chi}^2 = 9.1$), with no individual windows achieving excellent agreement with gufm1 and good agreement in only 3% of the windows. Model E fares worst ($\bar{\chi}^2 = 11.7$), with no windows that achieve even good agreement. If we adopt the advection time scale to renormalise our simulations, the number of gufm1-length windows in each run is different; however, we again find that model S much more frequently matches the observed character of the historical field.

The contribution of each criterion to the total misfit is designated by the different coloured areas in the time series plotted in figure 2. The total misfit of models W and E are often dominated by contributions from FCF (note the predominance of the red bands in panels a and b). Conversely, for model S no individual criterion tends to dominate the total misfit. For all three models, the time-average field from windows with particularly large FCF misfits often show high-latitude flux patches that are of the expected geographic extent, but that are exceptionally strong; rather than a preponderance of small yet intense flux patches.

Although model S best matches the global characteristics of gufm1 field structure, this model also has a very clear preference for concentration of high-latitude flux into a single pair of patches at American longitudes, as opposed to the two pairs of patches seen in gufm1. The FCF measure of Christensen et al. (2010) was specifically designed to ignore the longitudinal location of flux concentration as it was intended to be applied to simulations with homogeneous boundary conditions. In such cases the resultant longitudinal positions have no inherent meaning. However, with heterogeneous boundary conditions designed to match seismic constraints, as in this study, the resultant model longitudes are directly relatable to the Earth. Therefore, in order to investigate the tendency of ICB forcing in our simulations to concentrate flux in two patches at American longitudes we consider two new criteria that measure the flux balance between eastern and western hemisphere.

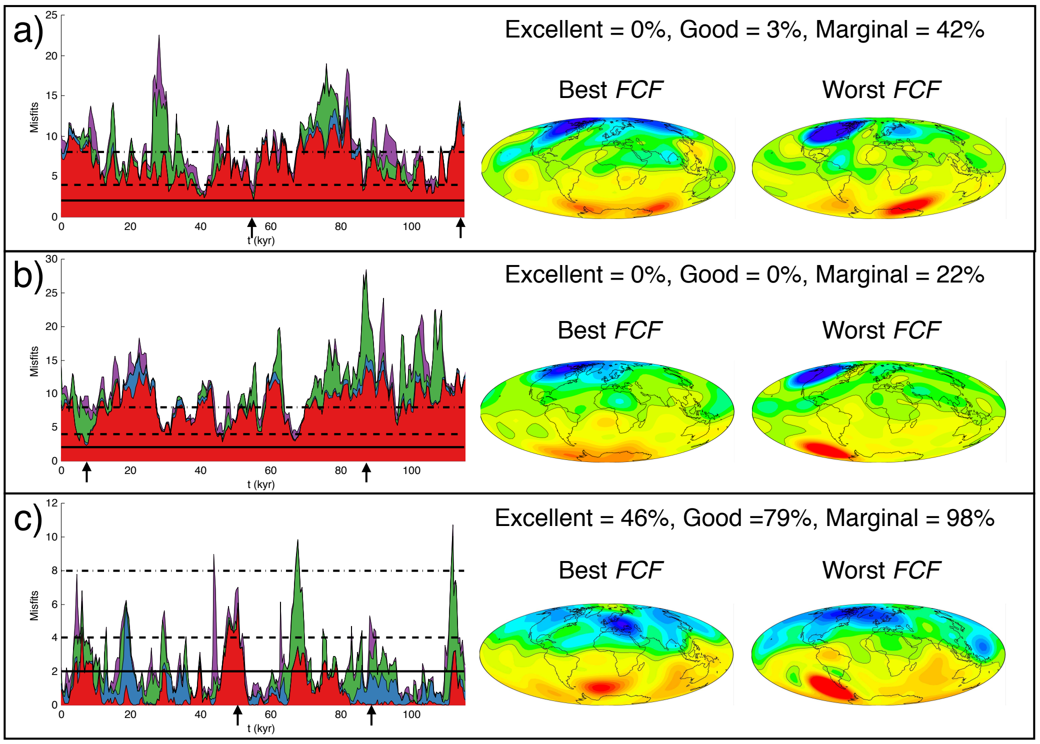

Figure 2: Agreement with observations for the the dynamo models with q_{i}^{*} equal to a) 0.023 (model W), b) 0.23 (model E), and c) 4.2 (model S), all other parameters as in Table 1. The coloured regions show the contributions from individual Christensen criteria: red = FCF, blue = AD/NAD, green = O/E, purple = Z/NZ. Horizontal lines indicate the misfit required for excellent (solid), good (dashed) and marginal (dash-dotted) agreement. Arrows below the time axis indicate the the times of the presented examples of the field for each model, times are correspond to the windows that provide the best and worst match to gufm1 according to only the FCF criterion.

We divide the CMB into 'high-latitude quadrants' bounded by the 0° and 180° lines of longitude, the north/south pole and the 30° lines of latitude. Within each quadrant we evaluate the Christensen flux concentration factor (FCF) and the total integrated flux

$$\mathrm{F} = \iint B_r \, dS \, . \tag{5}$$

For both FCF and F the field is truncated at spherical harmonic degree eight, and we evaluate the surface integrals numerically using Lebedev quadrature (Lebedev, 1976). The measures for each quadrant are then divided by the value obtained by considering only the axial dipole component of the field to produce normalised measures denoted FCF* and F*. This normalisation accounts for the contribution of the dipole component of the field to high latitude flux and hence the variations in the measures that could arise from changes in dipole intensity rather than redistribution of smaller scale features in the field.

The two measures provide complementary information on the structure of the field. The flux concentration factor FCF* depends on even powers of B_r, and thus measures the 'patchiness' of the field but does not distinguish between patches of normal or reversed flux. Integrating B_r results in cancellation of normal and reversed flux patches within a quadrant, although a large value of F* does not guarantee flux is concentrated into patches. Using both measures means that not only can the strength of flux concentration be measured, but we can distinguish between the influence of normal and reversed flux patches. The construction of the quadrants is also motivated to enable comparison with the high-latitude flux patches at American and Australasian longitudes that are clearly present in gufm1, as well as the general hemispheric balance of the field.

The normalised values (FCF*, F*) in the four quadrants (northwest, southwest, northeast, southeast) are combined to produce a measure of the hemispheric difference in high-latitude flux concentration,

$$H_{\mathrm{FCF}^*}, H_{\mathrm{F}^*} = \frac{(Q^*_{\mathrm{NW}} + Q^*_{\mathrm{SW}}) - (Q^*_{\mathrm{NE}} + Q^*_{\mathrm{SE}})}{(Q^*_{\mathrm{NW}} + Q^*_{\mathrm{SW}}) + (Q^*_{\mathrm{NE}} + Q^*_{\mathrm{SE}})}\,, \tag{6}$$

where Q^* stands for the relevant quadrant value. These measures of hemispheric bias are analogous to that used by Dietrich and Wicht (2013) for describing the hemispheric field structure of Mars. The measures are bounded by ± 1 and equal to zero if east and west are equal.

The evolution of FCF* and F* in the four quadrants over the duration of gufm1 is shown in figure 3. The most noticeable feature is the monotonic increase in the value of FCF* in the southwest quadrant (red line, panel a), accompanied by a monotonic decrease in F* within that quadrant (red line, panel b). These changes reflect the growth of the reverse flux patch at the CMB that produces the South Atlantic Anomaly (SAA), the field within the southwest quadrant becomes patchier through time but the total integrated flux decreases. Within gufm1 the northern high-latitude flux patches are less prominent at the earliest times, which may well reflect limitations in the data coverage rather than a change in field structure. Within the gufm1 reconstruction the intensity of the northwestern patch increases approximately a century before that of the northeastern patch and this timing difference is clearly visible in the evolution of FCF* in the relevant quadrants.

We are particularly interested in the hemispheric balance of the field, and the evolution of the relevant measures ($H_{\mathrm{FCF}^*}, H_{\mathrm{F}^*}$) are plotted as a phase diagram (panel c of figure 3). Each blue dot in this figure represent an individual snapshot from gufm1, with the most recent times residing within the upper-left region of this phase diagram. The present-day magnetic field in the high latitudes of the western hemisphere is patchier than in the eastern hemisphere ($H_{\mathrm{FCF}^*} > 0$) but with less total flux ($H_{\mathrm{F}^*} < 0$), again reflecting the influence of the SAA reverse flux patch. The magnetic field evolves over the course of gufm1, but on average the concentration of flux is nearly balanced between eastern and western hemispheres (red square, panel c).

We also consider the evolution of the hemispheric distribution of flux patches throughout CALS10k.1b in figure 3, panel d. In this case we truncate the model at spherical harmonic degree 4 as the field is less well constrained over the Holocene than in the historical model of gufm1. The hemispheric pattern of individual snapshots from CALS10k.1b is generally biased slightly towards more flux in the west, but with more patchiness in the east; the present field configuration of more flux in the east, but patchier in the west, appears unusual within the Holocene. The present field configuration may not be unusual as it is possible that the geographic distributions of the data used may result in CALS10k.1b not adequately capturing the hemispheric balance of the Earth's field throughout the model. It is also possible that the length of CALS10k.1b is insufficient to establish the long-term hemispheric balance of the Earth's field. The hemispheric balance in our dynamo models varies considerably through time (figure 4), and we find that if we consider the progressive running average of the hemispheric measures it takes approximately 25,000 model years to accurately determine the final time-averaged field morphology. This is similar to the timescale found by Davies and Constable (2014) for the non-zonal components of the field to converge on their

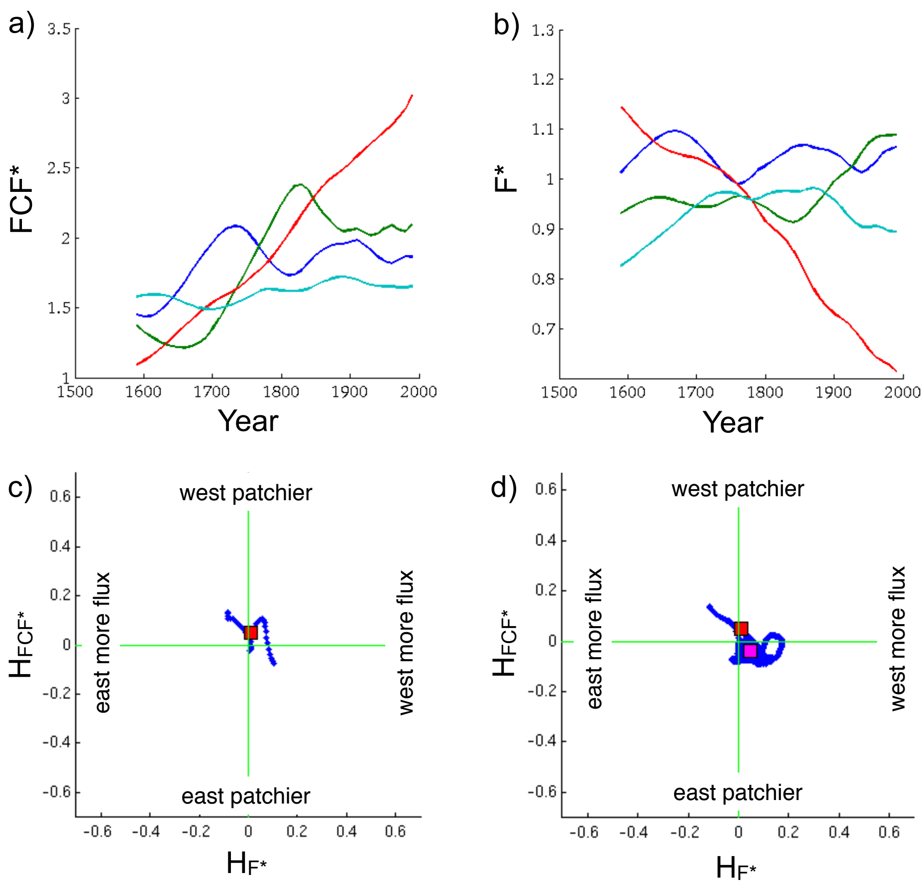

Figure 3: Flux concentration in observational models. Evolution of the a) FCF* measure and b) F* measure through time in gufm1 in the northwest (blue), northeast (green), southwest (red) and southeast (cyan) quadrants. Hemispheric measures through time: c) blue dots are values for individual snapshots from gufm1, the red square is the average of all snapshots; d) blue dots are values for individual snapshots from CALS10k.1b, the magenta square is the average of all snapshots, the red square is the gufm1 average for comparison.

long-term averages.

Phase diagrams showing the hemispheric balance of flux in our three dynamo models are shown in figure 4; note that in this case each individual dot represents the average over a window spanning 400 model years. The models show a great deal of variability in their east-west flux balance and can reach rather large values of hemispheric disparity; for example, model E contains windows in which H_{F^*} exceeds 0.6, implying that the sum of F^* in the western quadrants is more than four times greater than in the eastern quadrants. For our simulations, model W has the average hemispheric balance that is most similar to that of gufm1; as q_{i}^* is increased in the models there is an increasing tendency for flux to be concentrated in the west and model S is dominated by fields in which both H_{FCF^*} and H_{F^*} are positive. The magnetic fields of all three models are highly variable through time, showing a much greater range of values in their 400-year window averages, than either gufm1 or CALS10k.1b showed in their individual snapshots. Although a definitive long-term time-average requires approximately 25,000 model years to obtain, the preference for the patches of strong flux to form at American longitudes in model S is clear not only in the long-term time average but also in the majority of individual 400-year windows; only $\sim 1\%$ of windows have $H_{\mathrm{F}^*} < 0$ in this model.

3.2. Secular Variation

We also compare our dynamo models to the pronounced quiet Pacific secular variation observed in the modern field. To define our measure of Pacific SV quietness we first define the secular variation density within a

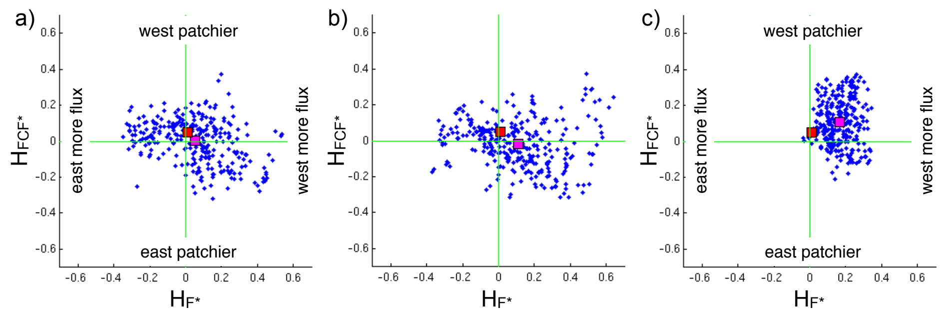

Figure 4: Dynamo model flux concentrations. Hemispheric measures of FCF* and F* through time for the models with q_i^* equal to a) 0.023 (model W), b) 0.23 (model E), and c) 4.2 (model S); blue dots are values for individual 400-year windows, the pink square is the average of all windows, the red square is the average of gufm1.

given region as

$$\rho_{\rm SV} = < |\dot{B}_r| > , \tag{7}$$

where the time derivative of the radial field is evaluated on the CMB. For convenience we define 'the Pacific' as either the hemisphere between 90°E and 90°W, or by the more restricted region bounded by 50°S, 50°N, 135°E and 90°W. Similar to our measures of hemispheric flux concentration, we construct a measure of Pacific SV quietness by comparing the secular variation density within the Pacific ($\rho_{SV}^{\rm p}$) to that in the rest of the world ($\rho_{SV}^{\rm np}$) as defined by

$$H_\rho = \frac{\rho_{SV}^{\rm p} - \rho_{SV}^{\rm np}}{\rho_{SV}^{\rm p} + \rho_{SV}^{\rm np}} \, . \tag{8}$$

This measure is zero when ρ_{SV} is equal within and outside the Pacific, is bounded by ±1, and is positive/negative when the Pacific is noisy/quiet.

We evaluate the average and standard deviation of H_ρ over the duration of both our numerical simulations and selected observational models of the geomagnetic field (figure 5). The reduced temporal and spatial resolution at early times in gufm1 and the Holocene models means that in these cases the resultant estimates of secular variation are not directly comparable to the effectively instantaneous SV determinations that are possible for the present field and our geodynamo models. However, changes in the spatial structure of the magnetic field through time in these models must ultimately reflect the accumulated action of an underlying pattern of secular variation and thus provide some insight into the persistence of the quiet Pacific. When evaluating H_ρ for our simulations and the modern field models we truncate at spherical harmonic degree 8, for the Holocene models we truncate at degree 4.

The modern magnetic field, as described by the CHAOS4 model, clearly has quiet Pacific secular variation, particularly if we consider our more restricted region rather than the hemispheric balance. The Pacific is quiet throughout gufm1, with the value of H_ρ based on the more restricted region being more variable than the hemispheric H_ρ, but the two measures result in very similar averages ($\bar{H}_\rho = -0.24 \pm 0.07$ or $\bar{H}_\rho = -0.26 \pm 0.13$). H_ρ varies considerably in the Holocene models, with an average value of approximately zero. There are times when large changes in the magnetic field are seen over the Pacific, as well as times during which the Pacific field is relatively steady. Although not as well constrained as gufm1, the Holocene models suggest that the quiet Pacific may not be representative of the Earth's field over long time scales.

Similar to the Holocene models, H_ρ varies considerably in our geodynamo models, with all three models showing times of both quiet and noisy Pacific SV. We consider our simulations to have an excellent, good or marginal

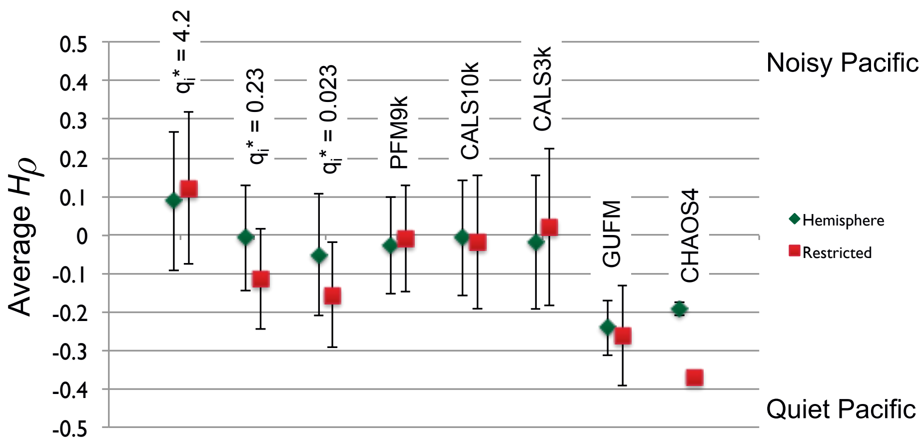

Figure 5: Quietness of Pacific secular variation for different field models computed using hemispheres (green) and our more restricted Pacific region (red). Error bars represent one standard deviation in the values of H_ρ based on the sampling interval of the given model.

match to the Earth's SV when $\bar{H}_\rho$ over the 400-year window is within one, two or four standard deviations of the gufm1 value, respectively. As q_{i}^* is increased in our models there is a trend towards noisier Pacific SV, resulting in an increase in the time-averaged value of H_ρ (figure 5). All three models sometimes produce 400-year windows with average H_ρ values that match gufm1; however, such windows are more common in model W. The preference for patches of strong flux to be located at American longitudes in model S means that changes in those patches also results in localisation of regions of high SV at American longitudes, and hence the western hemisphere, for that model.

In figure 6 we consider the overall match of our simulations to the observed properties of gufm1 based on six characteristics. Misfit to the morphology of the field, excluding flux concentration, is measured by the Christensen

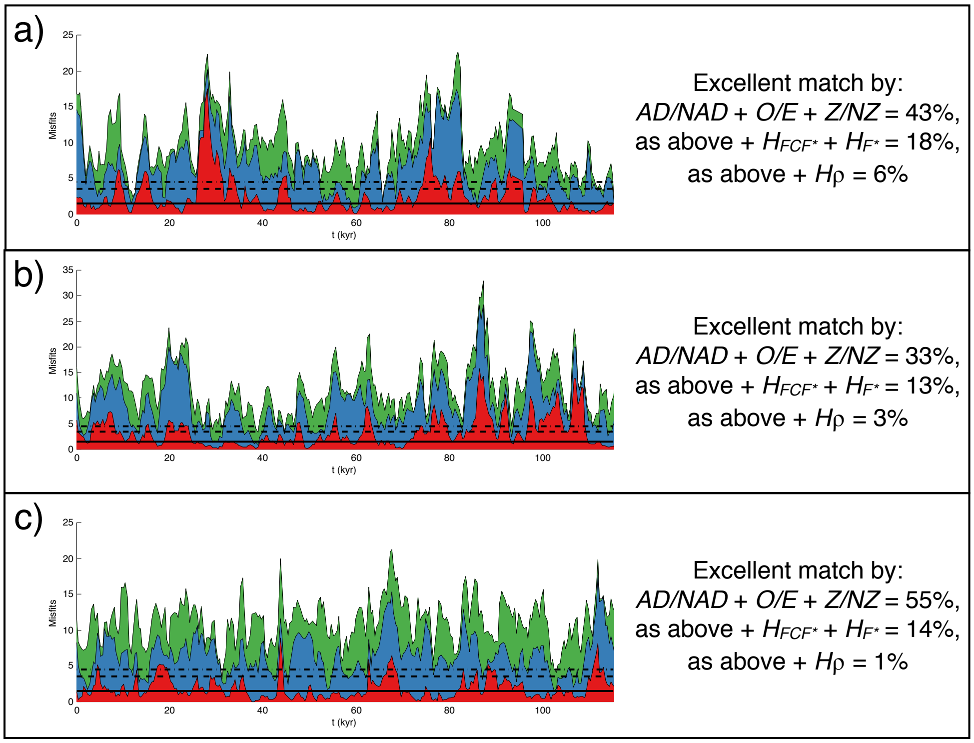

Figure 6: Misfit between 400-year windows from the dynamo models and gufm1 as determined by a combination of the Christensen criteria and our new measures, for models with q_i^* equal to a) 0.023 (model W), b) 0.23 (model E), and c) 4.2 (model S). The red area show the misfit contribution from $AD/NAD + O/E + Z/NZ$, the blue area shows the misfit contribution from $H_{\mathrm{FCF}^*} + H_{\mathrm{F}^*}$, and the green area the misfit contribution from H_ρ. Horizontal lines show the misfit levels required for excellent agreement based on the 'red' criteria (solid), the 'red' plus 'blue' criteria (dashed), the 'red' plus 'blue' plus 'green' criteria (dash-dotted).

criteria AD/NAD, O/E and Z/NZ, and indicated by the red bands. Misfit to the flux concentration is measured by H_{FCF^*} and H_{F^*}, and indicated by the blue bands. Misfit to the quiet Pacific secular variation is measured by H_ρ, and indicated by the green bands. All models occasionally, although rarely, have excellent matches to the total misfit based on both field and SV structure. Model S most frequently matches the field morphology of gufm1, as measured by the three Christensen criteria; however, it least frequently manages an excellent match to all six criteria simultaneously. The propensity for our strong ICB heterogeneity to concentrate flux and SV at American longitudes means that it only rarely matches the hemispheric balance of the field in gufm1.

4. Discussion

Hemispheric heat flux boundary conditions applied at the ICB can have a detectable influence on the structure and secular variation of the magnetic field, even in the presence of strong heterogeneity in CMB heat flux. Strong ICB heterogeneity promotes the existence of a single pair of high latitude patches of anomalously intense flux when the field is averaged over a sufficiently long time. This flux concentration is located at American longitudes in our models; however, previous simulations of non-magnetic convection (Davies et al., 2013) found that the location of upwelling and downwelling flows below the CMB varied with both Ra and q_{i}^*. Therefore, we expect the location of the downwelling flow in dynamo models, and the longitude of any resultant flux and SV concentrations, will also depend on the particular combination of model parameters chosen. Regardless of the exact longitudinal placement of the flux patches, a persistent hemispheric bias in core flow and hence the geomagnetic field and its secular variation represents an observational signature of inner core translation.

Increasing q_{i}^* in our simulations results in a model field that matches the structure of the gufm1 magnetic field more frequently, compared to models with weaker ICB heterogeneity, as measured by the global morphological criteria of Christensen et al. (2010). When ICB heterogeneity is weak the model produces a preference for quiet SV within the Pacific, conversely there is a preference for Pacific SV to be noisy when ICB heterogeneity is increased. This trend in $\bar{H}_\rho$ is caused by the tendency for strong SV to be associated with the high-latitude flux patches that preferentially develop at American longitudes in the time average of our model with strong ICB heterogeneity. In contrast, the time-averaged flow in our model with weak ICB heterogeneity is strongly influenced by the imposed CMB heat flux variations which tends to promote quiet Pacific SV.

The field and SV characteristics of all three dynamo models vary considerably through time. All models occassionally produce 400-year windows that simultaneously meet our criteria for excellent agreement with both the gufm1 field and SV. Measurement with the Christensen FCF criteria indicate that the model with strong ICB heterogeneity best matches the Earth's flux concentration, despite a pronounced preference for flux patches at American longitudes that is not apparent in gufm1. We therefore consider new criteria that measure the hemispheric bias of the field. These measures show that all three simulations sometimes produced fields with very strong hemispheric biases, with an overall bias towards the west becoming more pronounced as

ICB heterogeneity strength increases.

The previous work of Aubert et al. (2013) preferred a more moderate value of q_i^*, similar to our model E, which we do not find to be associated with a strong hemispheric bias. This difference may result from our adoption of no-slip conditions at both the inner and outer boundary, whereas their work had a free-slip condition at the outer boundary. As in the study of Aubert et al. (2013) we assume that the orientation of the ICB heterogeneity remains fixed through time as differential rotation of the inner core with respect to the mantle would preclude a longitudinal structure in the long-term time average. However, in contrast with the preferred model of Aubert et al. (2013), which had enhanced ICB heat flux in the eastern hemisphere, our models have enhanced heat flux in the western hemisphere of the ICB. The seismic observations establish a pattern of inner core heterogeneity, but interpretation of these results in terms of proposed mechanisms of inner core growth can suggest either melting in the west or melting in the east (Monnereau et al., 2010; Cormier et al., 2011), and Aubert et al. (2013) argue that the geomagnetic observations require enhanced heat flux (i.e., solidification) in the east. Changing the orientation of the ICB heterogeneity in our models would alter the orientation of the observed geomagnetic hemispheric signal; however, our previous non-magnetic modelling (Davies et al., 2013) indicate that the orientation of hemispheric patterns of core flow are not simply related to the choice of control parameters. Given the sensitivity to control parameters and the inherent time variability of the models, caution must be exercised in considering any relation between the orientation of the ICB heterogeneity and the orientation of a geomagnetic hemispheric imbalance over a relatively short time window.

The time variability of the generated field in all of our simulations means that they often depart from both the field and SV characteristics of gufm1. We find that heterogeneous ICB forcing is not required for our simulations to produce windows spanning 400 model years that have a field and SV structure that matches gufm1. Although there is a weak ICB heterogeneity in model W, the CMB heterogeneity is more important in that model, and that model does sometimes produce magnetic fields similar to gufm1. However, it should be noted that gufm1 may not be typical of the longer-term average structure of the Earth's field, particularly for our measure of SV. The magnetic fields of our geodynamo models, and perhaps the Earth, only show the influence of boundary control in the time average. Individual snapshots of the field or SV can depart significantly from the average structure, which takes on the order of tens of thousands of years to be resolved in our models, when rescaled using τ^{d}. Use of τ^{a} to rescale time would bring this averaging time to just within the reach of current Holocene models. If a strong hemispheric imbalance of both field and SV is a persistent feature of the Earth's field, then an explanation involving hemispheric heterogeneity at the ICB does seem to be required.

The influence of the boundaries on dynamo action would change over geologically long timescales as the processes responsible for the boundary heterogeneity evolve. At the CMB, mantle convection will redistribute hot and cold material, altering both the pattern and amplitude of the heat flux heterogeneity. Any influence of ICB heterogeneity on outer core flow obviously would not exist prior to the formation of the inner core or the onset of inner core translation. Structures with a longitudinal preference that persist in the magnetic field over millions of years almost certainly require some form of boundary influence (e.g. Gubbins and Kelly, 1993; Olson and Deguen, 2012) as these timescales are much longer than any timescale expected for the internal dynamics of core convection (e.g. Hollerbach, 2003).

In gufm1 there are two pairs of strong flux patches in the time average, one at American and one at Australasian longitudes. In the time average of CALS10k.1b, only the American patch is evident in the northern hemisphere. In the southern hemisphere both patches are evident in the full time average of CALS10k.1b; however, if the average is restricted to times post-5000 BC the patch near South America is somewhat stronger than the patch near Australia (Korte et al., 2011). The time-averaged field of PFM9k.1 (Nilsson et al., 2014) also shows a preference for a relatively stronger patch at American longitudes in the souther hemisphere, but more of an east-west balance in the northern hemisphere patches. The density of observations at high-latitudes, particularly in the southern hemisphere, means that the flux patches are difficult to resolve (Nilsson et al., 2014); however, the Holocene models may suggest an east-west imbalance in flux concentration. Based on our results, such a hemispheric imbalance is not expected from the pattern of CMB heterogeneity, but does arise naturally from the imposed pattern of ICB heterogeneity. It is important to establish the robustness, and strength, of any hemispheric bias in the geomagnetic field from observations over multi-millennial timescales in order to better constrain the relative importances of ICB and CMB heat flux heterogeneity on the dynamics of the outer core.

5. Acknowledgments

C.D. received support for this work from a Natural Environment Research Council personal fellowship, NE/H01571X/1. J.M. and L.S. received funding from the Natural Environment Research Council through Grant NE/G002223/1. This work made use of the facilities of HECToR, the UK's national high-performance computing service, which was provided by UoE HPCx Ltd at the University of Edinburgh, Cray Inc and NAG Ltd, and funded by the Office of Science and Technology through EPSRC's High End Computing Programme. We thank Julien Aubert and an anonymous reviewer for their useful comments.

Alboussière, T., Deguen, R., Melzani, M., 2010. Melting-induced stratification above the Earth's inner core due to convective translation. Nature 466 (7307), 744–747.

Aubert, J., Finlay, C. C., Fournier, A., 2013. Bottom-up control of geomagnetic secular variation by the Earth's inner core. Nature 502 (7470), 219–223.

Bloxham, J., 2000. The effect of thermal core-mantle interactions on the palaeomagnetic secular variation. Philosophical Transactions of the Royal Society of London. Series A: Mathematical, Physical and Engineering Sciences 358 (1768), 1171–1179.

Christensen, U. R., Aubert, J., Hulot, G., 2010. Conditions for Earth-like geodynamo models. Earth and Planetary Science Letters 296 (3-4), 487–496.

Cormier, V. F., Attanayake, J., He, K., Oct. 2011. Inner core freezing and melting: Constraints from seismic body waves. Physics of the Earth and Planetary Interiors 188 (3-4), 163–172.

Davies, C. J., Constable, C. G., 2014. Insights from geodynamo simulations into long-term geomagnetic field behaviour. Earth and Planetary Science Letters 404, 238–249.

Davies, C. J., Silva, L., Mound, J., 2013. On the influence of a translating inner core in models of outer core convection. Physics of the Earth and Planetary Interiors 214 (C), 104–114.

Deguen, R., Alboussiere, T., Cardin, P., 2013. Thermal convection in Earth's inner core with phase change at its boundary. Geophysical Journal of the Royal Astronomical Society 194 (3), 1310–1334.

Dietrich, W., Wicht, J., 2013. A hemispherical dynamo model: Implications for the Martian crustal magnetization. Physics of the Earth and Planetary Interiors 217 (C), 10–21.

Gibbons, S. J., Gubbins, D., 2000. Convection in the Earth's core driven by lateral variations in the core–mantle boundary heat flux. Geophysical Journal of the Royal Astronomical Society 142 (2), 631–642.

Gubbins, D., Alfè, D., Davies, C. J., 2013. Compositional instability of Earth's solid inner core. Geophysical Research Letters, 40, 1–5.

Gubbins, D., Kelly, P., 1993. Persistent patterns in the geomagnetic field over the past 2.5 Myr. Nature 365, 829–832.

Gubbins, D., Willis, A. P., Sreenivasan, B., 2007. Correlation of Earth's magnetic field with lower mantle thermal and seismic structure. Physics of the Earth and Planetary Interiors 162 (3-4), 256–260.

Hollerbach, R., 2003. The range of timescales on which the geodynamo operates. Earth's core: dynamics, structure, rotation, 181–192.

Jackson, A., Jonkers, A., Walker, M., 2000. Four centuries of geomagnetic secular variation from historical records. Philosophical Transactions of the Royal Society of London. Series A: Mathematical, Physical and Engineering Sciences 358 (1768), 957–990.

Korte, M., Constable, C., 2011. Improving geomagnetic field reconstructions for 0–3 ka. Physics of the Earth and Planetary Interiors 188 (3-4), 247–259.

Korte, M., Constable, C., Donadini, F., Holme, R., 2011. Reconstructing the Holocene geomagnetic field. Earth and Planetary Science Letters 312 (3-4), 497–505.

Labrosse, S., 2014. Thermal and compositional stratificaion of the inner core. Comptes Rendus Geoscience 346 (5-6), 119–129.

Lebedev, V. I., 1976. Quadratures on a sphere. USSR Computational Mathematics and Mathematical Physics 16 (2), 10–24.

Masters, G., Johnson, S., Laske, G., Bolton, H., Davies, J. H., 1996. A Shear-Velocity Model of the Mantle [and Discussion]. Philosophical Transactions of the Royal Society A: Mathematical, Physical and Engineering Sciences 354 (1711), 1385–1411.

Miller, M. S., Niu, F., Vanacore, E. A., 2013. Aspherical structural heterogeneity within the uppermost inner core: Insights into the hemispherical boundaries and core formation. Physics of the Earth and Planetary Interiors 223 (C), 8–20.

Monnereau, M., Calvet, M., Margerin, L., Souriau, A., 2010. Lopsided Growth of Earth's Inner Core. Science 328 (5981), 1014–1017.

Nakagawa, T., Tackley, P. J., 2008. Lateral variations in CMB heat flux and deep mantle seismic velocity caused by a thermal–chemical-phase boundary layer in 3D spherical convection. Earth and Planetary Science Letters 271 (1-4), 348–358.

Nilsson, A., Holme, R., Korte, M., Suttie, N., Hill, M., 2014. Reconstructing Holocene geomagnetic field variation: new methods, models and implications. Geophysical Journal International 198, 229–248.

Niu, F., Wen, L., 2001. Hemispherical variations in seismic velocity at the top of the Earth's inner core. Nature 410 (6832), 1081–1084.

Olsen, N., Lühr, H., Finlay, C. C., Sabaka, T. J., Michaelis, I., Rauberg, J., Tøffner-Clausen, L., 2014. The CHAOS-4 geomagnetic field model. Geophysical Journal International 197, 815–827.

Olson, P., Christensen, U. R., 2002. The time-averaged magnetic field in numerical dynamos with non-uniform boundary heat flow. Geophysical Journal International 151, 809–823.

Olson, P., Deguen, R., 2012. Eccentricity of the geomagnetic dipole caused by lopsided inner core growth. Nature Geoscience 5 (8), 565–569.

Olson, P. L., Christensen, U. R., Driscoll, P. E., 2012. From superchrons to secular variation: A broadband dynamo frequency spectrum for the geomagnetic dipole. Earth and Planetary Science Letters 319-320 (C), 75–82.

Pozzo, M., Davies, C., Gubbins, D., Alfè, D., 2014. Thermal and electrical conductivity of solid iron and iron–silicon mixtures at Earth's core conditions. Earth and Planetary Science Letters 393 (C), 159–164.

Sasaki, Y., Takehiro, S.-i., Nishizawa, S., Hayashi, Y.-Y., 2013. Effects of latitudinally heterogeneous buoyancy flux conditions at the inner core boundary of an MHD dynamo in a rotating spherical shell. Physics of the Earth and Planetary Interiors 223 (C), 55–61.

Tanaka, S., Hamaguchi, H., 1997. Degree one heterogeneity and hemispherical variation of anisotropy in the inner core from PKP (BC)–PKP (DF) times. Journal of Geophysical Research: Solid Earth (1978–2012) 102 (B2), 2925–2938.

Waszek, L., Deuss, A., 2011. Distinct layering in the hemispherical seismic velocity structure of Earth's upper inner core. Journal of Geophysical Research: Solid Earth (1978–2012) 116 (B12).

Willis, A. P., Sreenivasan, B., Gubbins, D., 2007. Thermal core–mantle interaction: Exploring regimes for 'locked' dynamo action. Physics of the Earth and Planetary Interiors 165 (1-2), 83–92.